Liver overexpression of PDGF-AA impairs insulin signaling in diabetes

Amar Abderrahmani[1,2*], Loïc Yengo[1*], Robert Caiazzo[3*], Mickaël Canouil[1*], Stéphane Cauchi[1], Violeta Raverdy[3], Valérie Plaisance[1], Valérie Pawlowski[1], Stéphane Lobbens[1], Julie Maillet[1], Laure Rolland[1], Raphael Boutry[1], Maxime Kwapich[1], Mathie Tenenbaum[1], Julien Bricambert[1], Sophie Saussenthaler[4], Elodie Anthony [5], Pooja Jha[6], Julien Derop[1], Olivier Sand[1], Iandry Rabearivelo[1], Audrey Leloire[1], Marie Pigeyre[3], Martine Daujat-Chavanieu[7], Sabine Gerbal-Chaloin[7], Tasnim Dayeh[8], Guillaume Lassailly[9], Philippe Mathurin[9], Bart Staels[10], Johan Auwerx[6], Annette Schürmann[4], Catherine Postic[5], Clemens Schafmayer[11], Jochen Hampe[12], Amélie Bonnefond[1,2], François Pattou[3*], Philippe Froguel[1,2*]

[1]Univ. Lille, CNRS, Institut Pasteur de Lille, UMR 8199 - EGID, F-59000 Lille, France; [2]Department of genomics of common disease, Imperial College London, UK; [3]Univ. Lille, Inserm, CHU Lille, U1190 - EGID, F-59000 Lille, France; [4]Department of Experimental Diabetology, German Institute of Human Nutrition Potsdam-Rehbrüecke, Nuthetal and German Center for Diabetes Research (DZD), München-Neuherberg, Germany. [5]Inserm, U1016, Institut Cochin, Paris, France CNRS UMR 8104, Paris, France Université Paris Descartes, Sorbonne Paris Cité, Paris, France. [6]Laboratory of Integrative and Systems Physiology, École Polytechnique Fédérale de Lausanne, 1015 Lausanne, Switzerland. [7]INSERM U1183, Univ. Montpellier, UMR 1183, Institute for Regenerative Medicine and Biotherapy, CHU Montpellier, France; [8]Department of clinical science; Skane University Hospital Malmö, Malmö, Sweden; [9]Univ. Lille, Inserm, CHU Lille, U995 - LIRIC - Lille Inflammation Research International Center, F-59000 Lille, France; [10]Univ. Lille, Inserm, CHU Lille, Institut Pasteur de Lille, U1011- EGID, F-59000 Lille, France; [11] Department of Visceral and Thoracic Surgery,

University Hospital Schleswig-Holstein, Kiel, Germany; [12]Medical Department 1, Technische Universität Dresden (TU Dresden), Dresden, Germany.

*These authors equally contributed to the study

Corresponding authors:

Philippe Froguel, MD, PhD, p.froguel@imperial.ac.uk, and Amar Abderrahmani, PhD, amar.abderrahmani@univ-lille2.fr

Summary

Type 2 diabetes (T2D) is closely linked with non-alcoholic fatty liver disease (NAFLD) and hepatic insulin resistance, but the mechanisms of this interaction are still elusive. In the liver from obese individuals, we found that decreased methylation level of a CpG site in *PDGFA* (encoding platelet derived growth factor alpha known as a hepatic fibrosis marker) was associated with T2D risk, increased *PDGFA* expression, increased systemic insulin resistance and increased steatohepatitis. Both genetic risk score (GRS) analysis and cell modeling using immortalized human hepatocytes pointed to a causative impact of high insulin levels on *PDGFA* hypomethylation and overexpression, and on PDGF-AA increased liver secretion. We found that insulin induced PDGF-AA contributes to insulin resistance through the reduction of IRS1 content and through PKCϴ and PKCε activation. Furthermore, hepatocyte insulin sensitivity was restored by PDGF-AA blocking antibodies, PDGF receptors inhibitors or metformin. Therefore, in T2D, the increased hepatic PDGF-AA signaling caused by hyperinsulinemia aggravates hepatocyte insulin resistance, opening new therapeutic avenues against T2D and NAFLD.

KEY WORDS: Type 2 diabetes, Obesity, Liver, DNA methylation, Cell models, Mouse models, Insulin resistance, Epigenetics

Introduction

Genome-wide association studies (GWAS) for type 2 diabetes (T2D) and related metabolic traits have identified many loci associated with the risk of T2D [1]. However, these loci only explain 15% of T2D inheritance, and they have hardly opened new insights into the pathophysiology of T2D and its related complications, e.g. non-alcoholic fatty liver disease (NAFLD) that hits >70% of diabetic patients [2]. Epigenetic alteration of DNA methylation in key metabolic tissues such as the liver may contribute to T2D inheritance, providing novel mechanisms linking the pathogenic environment with T2D and complications [3]. Recent DNA methylation studies in adipose tissue, muscle, pancreatic islets and liver from small size cohorts of subjects have reported differentially methylated genomic sites associated with T2D and/or obesity [4–6]. A recent large-scale epigenome-wide association study performed in blood DNA has identified many genomic sites differentially methylated according to the distribution of body mass index (BMI) which predicted future development of T2D [7].

We investigated both methylome and transcriptome in livers from obese subjects presenting with T2D or with normal glucose levels. We found that a CpG site in *PDGFA*, known as a fibrosis and cancer factor, was associated with T2D risk, *PDGFA* expression, insulin resistance and steatohepatitis (NASH). We demonstrated a causative effect of high insulin serum concentrations on the methylation of this CpG site. Our human cell and animal modeling data suggested that epigenetic changes and the subsequent dramatic increase in hepatic PDGF-AA secretion links chronic hyperinsulinemia to hepatocyte insulin resistance via a vicious autocrine negative feedback loop.

Liver epigenetic modification in T2D

The liver genome-wide methylome was assessed in 96 age- and BMI-matched obese women with T2D and 96 obese women with normal glucose levels (**Extended Data Table 1**). After adjustment for steatosis, we found that methylation at only one CpG site (cg14496282) within *PDGFA* (encoding platelet derived growth factor alpha) is genome-wide significantly associated with decreased T2D risk (β = -15.6 %; $p = 2.5\times10^{-8}$; **Fig. 1a and 1b**). We checked the methylation, at this CpG site, for possible confounding effects due to differences in cell composition [8] and observed consistent effects for T2D risk (β = -14.9 %; $p = 6.9\times10^{-7}$). The average DNA methylation at the cg14496282 was 41.3 % in women with T2D and 60.3 % in controls, which corresponds to a 1.46-fold decrease in the methylation level of the CpG site. We replicated this association in livers from 12 German cases with T2D and 53 German control subjects [9], where T2D risk was associated with decreased methylation level at cg14496282 site (β = -14.0 %; $p = 0.01$) (**Extended Data Table 2**). These data were also supported by a recent study showing a decrease in *PDGFA* methylation in livers from obese men with T2D compared to non-obese controls [10].

We next investigated whether the T2D-associated *PDGFA* cg14496282 hypomethylation was specific to the liver. To do so, we assessed the blood DNA methylome from 12 obese cases with T2D and 12 obese normal glucose controls presenting with extreme liver methylation levels at cg14496282. We found a significant correlation between methylation levels in blood and liver (r = 0.66; $p = 6.61\times10^{-4}$), and a slightly reduced methylation at the cg14496282 site (β = -1.4 %; $p = 0.01$) in blood of subjects with T2D when compared to controls. We also compared DNA methylation at cg14496282 in 43 liver and skeletal muscle samples from randomly selected of 192 participants, but we did not find any significant correlation ($p > 0.05$).

In the 192 obese liver samples, we next investigated *cis*-located genes (within 500 kb around cg14496282) that were differentially expressed between T2D cases and controls, and which mRNA expression correlated with DNA methylation at *PDGFA* cg14496282 site. Using a false discovery rate threshold of five percent for differential expression analysis and methylation-expression correlation analysis, we identified that methylation at cg14496282 is negatively associated with the expression of *PDGFA* in T2D cases and normal glucose controls ($p < 0.007$; **Table 1**).

Decreased NASH and insulin resistance with hypomethylated *PDGFA*

In normoglycemic obese controls, we next found that *PDGFA* cg14496282 methylation is significantly associated with decreased fasting serum insulin levels and decreased insulin resistance as modeled by the homeostasis model assessment index HOMA2-IR ($\beta = -1.45\times10^{-3}$, $p = 2.32\times10^{-3}$; and $\beta = -0.10$, $p = 4.93\times10^{-3}$, respectively; **Table 1**). In contrast, *PDGFA* liver expression was significantly associated with increased fasting serum insulin levels and increased insulin resistance ($\beta = 6.83\times10^{-3}$, $p = 9.49\times10^{-3}$; and $\beta = 0.53$, $p = 7.47\times10^{-3}$, respectively; **Table 1**). Furthermore, in subjects with T2D and in normoglycemic controls, we found that *PDGFA* cg14496282 methylation was significantly associated with decreased NASH risk ($p < 0.05$; **Table 1**), while *PDGFA* expression in the liver was associated with increased NASH risk ($p < 0.01$; **Table 1**). Furthermore, in patients with T2D, *PDGFA* cg14496282 methylation was significantly associated with decreased hepatic fibrosis, decreased alanine aminotransferase levels and decreased aspartate aminotransferase levels ($p < 0.05$; **Table 1**), while *PDGFA* expression in the liver was associated with increased hepatic fibrosis and increased liver enzyme levels ($p < 0.01$; **Table 1**). These results were in line with previous studies which showed that *PDGFA* cg14496282 hypomethylation is associated with

increased *PDGFA* liver expression in advanced *versus* mild human NAFLD [11,12]. Moreover, it has been previously demonstrated that the activation of PDGF receptor signaling stimulates hepatic stellate cells and thereby, promotes liver fibrosis [13–15]. Moreover, the overexpression of Pdgfa in mice liver was found to cause spontaneous liver fibrosis [16].

Insulin modifies *PDGFA* methylation and expression

Subsequently, we calculated a genetic risk score (GRS) as the sum of alleles increasing fasting insulin levels over 19 GWAS-identified single nucleotide polymorphisms (SNPs) [17], and found that this GRS is associated with decreased DNA methylation at cg14496282 (β = -1.05 % per allele; $p = 4\times10^{-3}$; **Extended Data Table 3**). This association remained significant when we analyzed T2D cases and controls separately (and then meta-analyzed) or when we adjusted for BMI, HDL cholesterol or triglycerides; these traits having a genetic overlap with fasting insulin [17]. These results strongly suggested that hyperinsulinemia (and the subsequent insulin resistance) contributes to decreased DNA methylation of *PDGFA* cg14496282. In contrast, the GRS including 24 SNPs associated with fasting glucose, the GRS including 65 SNPs associated with T2D and the GRS including 97 SNPs associated with BMI were not associated with cg14496282 methylation (**Extended Data Table 3**).

We then investigated the effect of hyperinsulinemia on the expression of *PDGFA* in liver cells. As the *PDGFA* cg14496282 site is not conserved between humans and mice [18], we used an *in vitro* model of human hepatocytes. We first confirmed the expression of *PDGFA* in freshly isolated primary human hepatocytes and immortalized human hepatocytes (IHH) cells (**Extended Data Fig. 1**). Moreover, IHH cells and primary human hepatocytes secreted PDGF-AA homodimer at comparable levels (**Fig. 2a**). Exposure of IHH cells to 100 nM human insulin for 24, 48 and 72 hours led to a two- to five-fold increase in *PDGFA* expression (**Fig. 2b**). The

stimulatory effect of insulin on *PDGFA* expression was significant as early as six hours post insulin treatment (**Fig. 2c**). Importantly, we showed in this model that the rise of *PDGFA* expression by insulin correlated with the hypomethylation of the *PDGFA* cg14496282 site (**Fig. 2d**).

Although the cg14496282 CpG site is not conserved in mice, we next investigated whether insulin stimulates the expression of *Pdgfa* in mice liver. We found that acute administration of insulin to normal mice activated Akt in the liver (**Extended Data Fig. 2**) and stimulated *Pdgfa* expression (**Fig. 2e**), which is in line with our data in humans. This result indicates that in mice other mechanisms that cg14496282 methylation levels contribute to the rise of *PDGFA* expression triggered by insulin.

Moreover, parallel to increased *PDGFA* expression, we found that the abundance of the encoded protein PDGF-AA homodimer increases in response to insulin via the canonical PI3K/AKT pathway (**Fig. 2f-g**). The PI3K inhibitor wortmannin abolished the insulin-mediated increase in *PDGFA* expression and PDGF-AA homodimer abundance (**Figs. 2g and 2h**). The increase in *PDGFA* expression by insulin was not the consequence of changes in the IHH cell number, as insulin treatment for 24 hours did not modify the cell number and viability (**Extended Data Fig. 4**). Collectively, our data strongly suggested that the increase in *PDGFA* expression by insulin involves the insulin receptor signaling. In support of this hypothesis, we found that the pharmacological inhibition of insulin growth 1 factor receptor (IGF1R) activity does not prevent the rise of *PDGFA* expression elicited by insulin (**Extended Data Fig. 3**).

The lipid accumulation caused by insulin treatment may account for the increase in *PDGFA* expression. Our results infirmed this hypothesis as we found similar intracellular neutral lipid levels in insulin-treated IHH cells *versus* control cells, and we showed that the chronic exposure of IHH cells with palmitate that affect insulin-induced AKT activation did

not modify *PDGFA* expression (**Extended Data Fig. 5**). Thus, altogether our data support a direct causative role of the insulin signaling in the expression of *PDGFA*.

PDGF-AA induces hepatic insulin resistance

We then hypothesized that the hepatic overproduction of PDGF-AA in response to chronic hyperinsulinemia may mediate hepatocyte insulin resistance via a negative autocrine feedback loop. Furthermore, it has been proposed that this growth factor may contribute to the induction of its own expression [19]. Such regulation may contribute to perpetuate PDGF-AA secretion and insulin resistance. This hypothesis would be in line with the increased liver *Pdgfa* expression that we identified in several insulin resistant mice models. Indeed, we found that *Pdgfa* expression is increased by 46 % in the liver from C57BL/6J (B6) mice that are susceptible to diet-induced obesity [20], as compared with control mice (i.e. that do not respond to a high-fat diet) (**Fig. 3a and 3b**). Similarly, we found that liver *Pdgfa* expression is increased in New Zealand obese (NZO) diabetes-prone females [21] (**Fig. 3c and 3d),** and in insulin resistant BXD mice fed a high-fat diet for 21 weeks when compared to control mice (**Fig. 3e**).

To investigate the negative role of PGDF-AA on the hepatocyte insulin signaling, we have first measured the PDGF-AA secretion in IHH cells cultured with insulin. We found that PDGF-AA protein concentration in the supernatant of IHH cells progressively increased in response to insulin reaching a two-fold increase after 24 hours of incubation (**Fig. 4a**). Importantly, PDGF-AA secretion from IHH cells cultured with insulin was associated with impaired AKT phosphorylation at residue serine 473 (**Fig. 4b**). In line with AKT activation pivotal role in glycogen synthesis [22], we found reduced insulin-induced glycogen production in human hepatocytes (**Fig. 4c).**

RNA sequencing of IHH cells treated or not with insulin for 24 hours revealed a profound dysregulation of expression of genes involved in both carbohydrate metabolism, inflammatory and insulin signaling pathways in response to insulin. Indeed, when we grew a network based on *PDGFA* through Ingenuity Pathway Analysis (IPA), we found a significant increase in the expression of genes of the VEGF and PDGF families, including as expected *PDGFA* (log2 Fold Change = 0.80; $p = 1.1\times10^{-11}$) (**Extended Data Fig. 6a and Extended Data Table 5**). Subsequently, we analyzed the diseases and/or functions highlighted by the insulin-evoked deregulated expressed genes in IHH cIRSells. Among the significant outputs, we found a network related to the metabolism of carbohydrates that includes *PDGFA* ($p = 1.2\times10^{-6}$; **Extended Data Fig. 6b, Extended Data Table 6**). We also identified in cells cultured with insulin a decrease in the expression of the insulin receptor substrate 1 (*IRS1*) gene (**Fig. 4d**, **Extended Data Fig. 6b and Extended Data Table 6**). The decreased IRS1 expression by insulin, confirmed by western blotting, was concomitant with the decrease of AKT activation (**Fig. 4e).** Defective IRS1 level can therefore account for the impaired insulin signaling caused by chronic hyperinsulinemia.

PDGF-AA over-secretion may have a direct causative role in the defective insulin signaling caused by chronic incubation with insulin. We found that the culture of IHH cells with PDGF-AA inhibits insulin-induced AKT activation (**Fig. 4f**). Importantly, the incubation of IHH cells with anti-PDGF-AA blocking antibodies counteracted the negative long-term effect of insulin on AKT phosphorylation (**Fig. 4g)**. We then investigated the mechanism whereby PDGF-AA inhibits insulin-induced AKT activation. Human hepatocytes express PDGF receptors (PDGFR) including PDGFRα and PDGFRβ that both bind PDGF-AA [13]. Since our IHH RNA sequencing revealed the expression of these receptors, we tested the role of PDGFR signaling using the PDGFR tyrosine kinase inhibitor Ki11502 [23]. Pre-treatment of IHH cells with Ki11502 efficiently antagonized the negative effect of chronic insulin on AKT

phosphorylation thus, confirming our results obtained with the anti-PDGF-AA blocking antibodies (**Fig. 4h**). The improvement of insulin signaling by Ki11502 was further associated with increased ability of insulin to stimulate glycogen synthesis (**Fig. 4i**). To further dissect the signaling pathways by which chronic insulin and PDGF-AA impair AKT activation, we performed a global measurement of serine/threonine protein kinases (STKs) using STK PamGene arrays consisting of 140 immobilized serine/threonine-containing peptides that are targets of most known kinases [24]. We looked for differential STK activity between control and IHH cells cultured with insulin for 24 hours. Peptides whose phosphorylation varied significantly between the two conditions were indicative of differential specific STK activities. This unbiased kinase analyses underscored significant differences in protein kinases C (PKCϴ and PKCε) activities (**Fig. 4j**). The activation of these two PKCs hampers insulin signaling in response to chronic hyperlipidemia [25–27]. Therefore, we treated IHH cells with phorbol 12-myristate 13-actetate (PMA), a potent activator of PKCs, and retrieved AKT inhibition (**Extended Data Fig. 7a**). PKCϴ and PKCε kinase activities are associated with the phosphorylation at their Serine 676 and Serine 729, respectively [28,29]. We found a striking phosphorylation of the two PKCs, which coincided with the decreased AKT phosphorylation in IHH cells cultured with insulin for 16 hrs or 24 hrs (**Fig. 4k**). The effect of insulin on the phosphorylation of the two kinases and IRS1 content is likely to rely on PDGF-AA, as the activation of PKCϴ and PKCε and the decrease of IRS1 were found in IHH cells that were exposed to the PDGF-AA for 24 h (**Fig. 4l and 4m).** The decrease of IRS1 by PDGF-AA may be independent of PKC activation as the PMA was unable to mimic the effect of the growth factor on the IRS1 content (**Extended Data Fig. 7b**).

Our data demonstrated that the culture of IHH cells with PDGF-AA stimulated *PDGFA* expression (**Fig. 4n**) and PDGF-AA secretion (**Extended Data Fig. 8**). This effect was mediated by PDGFR as the PDGFR inhibitor ki11502 prevented the rise of *PDGFA* mRNA of

cells exposed to either insulin or PDGF-AA (**Fig. 4n and 4o**). Induction of *PDGFA* by PDGF-AA may require PKC activation since PMA mimicked both insulin and PDGF-AA effects on the *PDGFA* mRNA (**Fig. 4p**) and inversely, the PKC inhibitor sotrastaurin [30], which inhibits PKCϴ and PKCε, alleviated the rise of *PDGFA* induced by insulin for 24 hr (**Fig. 4q**) and PDGF-AA (**Fig. 4r**). The most prescribed T2D drug metformin inhibits PKCε [31]. In line with this effect, we found that metformin also efficiently abolished the expression of insulin-induced *PDGFA* mRNA (**Fig. 4s**), protein content (**Fig. 4t**) and secretion (**Fig. 4u**).

Altogether, our data support a role for liver PDGF-AA in promoting liver insulin resistance via the decrease of IRS1 and the activation of both PKCϴ and PKCε. In T2D, insulin induced PDGF-AA stimulates its own expression, impairing further hepatocyte insulin signaling and possibly the hepatic fibrogenesis by activating hepatic stellate cells[13–15].

Discussion

GWAS only identified few genes involved in NAFLD [32] and the contribution of epigenetics to T2D liver dysfunction is still elusive. While we initially identified 381 differentially methylated sites in liver from T2D obese patients (**Extended Data Fig. 9**), after adjusting for liver steatosis, we only observed one genome-wide significant T2D differentially methylated DNA site, associated with the increase of *PDGFA* expression in cis. Elevated *PDGFA* expression was also reported in biliary atresia [33], and is a diagnostic and prognostic biomarker of cholangiocarcinoma, a liver cancer of increased incidence that is not associated with obesity but with severe insulin resistance [34,35]. Notably, we found that liver *PDGFA* cg14496282 hypomethylation and concomitant rise in liver *PDGFA* expression were associated with systemic insulin resistance in non-diabetic obese patients but not with their glucose values.

The genetic data from our analysis of GRS related to insulin resistance, together with our in *vitro* and in *vivo* mice experiments, suggested a causative effect of insulin on methylation level, hepatic expression and secretion of this growth factor. *PDGFA* encodes a dimer disulfide-linked polypeptide (PDGF-AA) that plays a crucial role in organogenesis [36]. The activation of the PDGF-AA receptor signaling is involved in cirrhotic liver regeneration [37] and the chronic elevation of PDGF-AA in mice liver induces fibrosis [38]. The association of increased *PDGFA* expression with liver steatosis and fibrosis observed in our study and in others [11,12,39], supports a similar fibrogenic role in human liver, in which chronic hyperinsulinemia might be instrumental [40]. How prolonged hyperinsulinemia hampers downstream glucose metabolism in hepatocyte is still elusive, although a desensitization mechanism operating at the insulin receptor and IRS levels is likely [41]. We believe that PDGF-AA may contribute to the inhibitory effect of chronic hyperinsulinemia on hepatocyte insulin signaling via a feedback autocrine loop (**Fig. 5**). While the insulin signaling is required for stimulating the PDGFA expression, PDGF-AA stimulates its induction via the activation of PKC. This vicious cycle perpetuates

high PDGF-AA level and thereby continuous insulin resistance. Our data further suggested that the negative effect of PDGF-AA on insulin signaling is mediated through the decrease of IRS1 and PKC activation including PKCϴ and PKCε. These two kinases are known to phosphorylate IRS-1 and the insulin receptor on serine residues, that impairs the association of the insulin receptor with IRS proteins, leading to the blockade of AKT activation and of the downstream signaling [26,27].

Our findings may have a major interest for the treatment of T2D and of its hepatic complications. We showed that metformin, the most-widely prescribed oral insulin sensitizer agent prevented the PDGF-AA insulin-induced vicious circle. Metformin has been specifically proposed for diabetic patients with NAFLD and hepatocarcinoma (HCC) [42]. Metformin reduces the risk of HCC incidence in diabetic patients in a dose-dependent manner [43]. Thereby metformin may improve liver insulin sensitivity at least in part through PDGF-AA liver blockade, explaining its long-term effect against HCC. Beside liver insulin sensitizers, blocking PDGF-AA activity may be a promising alternative anti-diabetic therapeutic. The anti-tumor PDGFR inhibitor imatinib demonstrated unexpected (and unexplained until now) improvement of insulin sensitivity in insulin-resistant rats [44] as well as a dramatic blood-glucose-lowering effect in diabetic subjects treated for leukemia [45,46].

Our study also demonstrated that the human epigenome analysis, when directly performed in disease-affected tissues is an efficient tool to make progress in the pathogenesis of common diseases. Furthermore, it opens avenues in the identification of new drug targets to combat T2D, and complications linked to insulin resistance, including NAFLD and cancer.

Methods

Discovery study. Liver biopsies were collected from 192 subjects from the French obesity surgery. Subjects included in the discovery study were participants of the ABOS ("*Atlas Biologique de l'Obésité Sévère*") cohort (ClinicalGov NCT01129297) including 750 morbidly obese subjects whose several tissues were collected during bariatric surgery [47]. All subjects were unrelated, women, above 35 years of age, of European origin verified by Principal Component Analysis (PCA) using SNPs on the Metabochip array, non-smoker, non-drinker, without any history of hepatitis, and without indications of liver damage in serological analysis (normal ranges of aspartate aminotransferase, alanine aminotransferase and gamma-glutamyl transpeptidase). Overall, 96 T2D cases and 96 normoglycemic participants were selected. Normoglycemia and T2D were defined using the World Health Organization/International Diabetes Federation 2006 criteria (Normoglycemia: fasting plasma glucose < 6.1 mmol/l or 2-h plasma glucose < 7.8 mmol/l; T2D: fasting plasma glucose ≥ 7 mmol/l or 2-h plasma glucose ≥ 11 mmol/l). Each participant of the ABOS cohort signed an informed consent. For calculation of intermediate metabolic traits **(**HOMA2-IR and HOMA2-B indexes), see **supplemental information**. All procedures were approved by local ethics committees. The main clinical characteristics were presented in **Extended Data Table 1.**

Replication study. The replication study was based on *in silico* data of liver samples analyzed by the Infinium HumanMethylation450 BeadChip, as previously reported [9]. Clinical characteristics were reported in **Extended Data Table 2**. Liver samples were obtained percutaneously from subjects undergoing liver biopsy for suspected nonalcoholic fatty liver disease or intraoperatively for assessment of liver histology. Normal control samples were

recruited from samples obtained for exclusion of liver malignancy during major oncological surgery. None of the normal control subjects underwent preoperative chemotherapy, and liver histology demonstrated absence of both cirrhosis and malignancy. Consenting subjects underwent a routine liver biopsy during bariatric surgery for assessment of liver affection. Biopsies were immediately frozen in liquid nitrogen, ensuring an *ex vivo* time of less than 40 seconds in all cases. A percutaneous follow-up biopsy was obtained in consenting bariatric patients five to nine months after surgery. Patients with evidence of viral hepatitis, hemochromatosis, or alcohol consumption greater than 20 g/day for women and 30 g/day for men were excluded. All patients provided written, informed consent. The study protocol was approved by the institutional review board (‘‘Ethikkommission der Medizinischen Fakultät der Universität Kiel,’’ D425/07, A111/99) before the beginning of the study.

Epigenome-wide DNA methylation profiling. The epigenome-wide analysis of DNA methylation was performed using the Infinium HumanMethylation450 BeadChip (Illumina, Inc., San Diego, CA, USA) which interrogates 482,421 CpG sites and 3,091 non-CpG sites covering 21,231 RefSeq genes [48]. We used 500ng of DNA from liver tissue for bisulfate conversion using the EZ DNA Methylation kit D5001 (Zymo Research, Orange, CA, USA) according to the manufacturer’s instructions. Bisulfite converted DNA was amplified, fragmented and hybridized to the BeadChips following the standard Infinium protocol. All the samples were randomized across the chips and analyzed on the same machine by the same technician to reduce batch effects. After single base extension and staining, the BeadChips were imaged with the Illumina iScan. Raw fluorescence intensities of the scanned images were extracted with the GenomeStudio (V2011.1) Methylation module (1.9.0) (Illumina). The fluorescence intensity ratio was used to calculate the β-value which corresponds to the methylation score for each analyzed site according to the following equation: β-

value = intensity of the Methylated allele (M) / (intensity of the Unmethylated allele (U) + intensity of the Methylated allele (M) + 100). DNA methylation β-values range from zero (completely unmethylated) to one (completely methylated). All samples had high bisulfite conversion efficiency (signal intensity >4000) and were included for further analysis based on GenomeStudio quality control steps where control probes for staining, hybridization, extension and specificity were examined. The intensity of both sample dependent and sample independent built in controls was checked for the red and green channels using GenomeStudio.

Microarray mRNA expression analysis. Transcriptome profiling was performed using the HumanHT-12 v4.0 Whole-Genome DASL HT Assay (Illumina). Total RNA was converted to cDNA using biotinylated oligo-dT18 and random nonamer primers, followed by immobilization to a streptavidin-coated solid support. The biotinylated cDNAs were then simultaneously annealed to a set of assay-specific oligonucleotides based on content derived from the National Center for Biotechnology Information (NCBI) Reference Sequence Database (release 98). The extension and ligation of the annealed oligonucleotides generate PCR templates that are then amplified using fluorescently-labeled (P1) and biotinylated (P2) universal primers. The labeled PCR products were captured on streptavidin paramagnetic beads, to yield single-stranded fluorescent molecules which were then hybridized, via gene-specific complementarity, to the HumanHT-12 BeadChip, thereafter fluorescence intensity was measured for each bead. Hybridized chips were scanned by using iScan (Illumina) and raw measurements were extracted by GenomeStudio software version 3.0 (Illumina).

SNP genotyping, ethnic characterization and genetic risk score. SNP genotyping was performed with Metabochip DNA arrays (custom iSelect-Illumina genotyping arrays) using the

Illumina HiScan technology and GenomeStudio software (Illumina, San Diego, CA, USA)[49]. We selected SNPs with a call rate ≥ 95 % and with no departures from Hardy–Weinberg equilibrium ($p>10^{-4}$). A Principal Component Analysis (PCA) was performed in a combined dataset involving the 192 patients plus 272 subjects from the publicly available HapMap project database. For these 272 subjects (87 of European ancestries [HapMap CEU], 97 of Asian ancestries [HapMap CHB] and 88 of African ancestries [HapMap YRI]) genotype calls at the 106,470 SNPs present on the Metabochip were available. The first two components were sufficient to discriminate ethnic origin (**Extended Data Fig. 10**) and we observed that study participants clustered well with HapMap samples of European ancestries. We used 19 SNPs previously established for their association with fasting insulin to assess the possibility of causal direct link between DNA methylation at cg14496282. These 19 SNPs were on the Metabochip and all passed our quality control. These SNPs as well as the associated insulin raising alleles are reported in **Extended Data Table 3**. We assessed the combined effect of these SNPs on DNA methylation using either fixed-effect meta-analysis and by testing the association of DNA methylation at cg14496282 with a genetic risk score (GRS) defined for each individual as the count of the number of fasting insulin raising alleles. We also tested the association between three other GRS (T2D, BMI and fasting glucose raising alleles) and DNA methylation at cg14496282 and expression (**Extended Data Table 4**).

Statistical Analyses. Statistical analysis and quality control were performed with R software version 3.1.1 [50]. Raw data (IDAT file format) from Infinium HumanMethylation450 BeadChips were imported into R using the *minfi* package (version 1.12.0 on Bioconductor) [51], then we applied the preprocessing method from GenomeStudio software (Illumina) using the reverse engineered function provided in the *minfi* package. Samples were excluded when less than 75 % of the markers had detection *p*-values below 10^{-16}. Markers were ruled out when less than 95

% of the samples had detection *p*-values below 10^{-16}. According to this strategy, no sample was excluded and 70,314 markers (over 485,512) were excluded. To correct for Infinium HumanMethylation450 BeadChip design which includes two probe types (Type I and Type II), a Beta-MIxture Quantile normalization (BMIQ) [52] was performed. Moreover, we checked for outliers using Principal Component Analysis (PCA) (*flashpcaR* package, version 1.6-2 on CRAN). At this stage, 416,693 markers and 192 samples were kept for further analysis. To test the association between methylation level and diabetic status, we applied a linear regression adjusted for steatosis (in percent), presence of NASH and fibrosis. Results were corrected for multiple testing using a Bonferroni correction ($p<10^{-7}$). The association between DNA methylation and metabolic traits was analyzed using a linear regression model, including normoglycemic samples adjusted for age and BMI. Quality control was performed on the HumanHT-12 v4.0 Whole-Genome DASL HT Assay (Illumina) data, according to the following criterion: probes were kept for further analysis when the detection *p*-values provided by GenomeStudio software version 3.0 (Illumina) were below five percent for all samples. A PCA was performed to identify samples with extreme transcriptomic profiles. After the quality control just described, 18,412 probes matching 13,664 genes and 187 samples were kept and analyzed for differential expression between T2D cases and controls, using linear regression. To account for multiple testing, we used five percent as a threshold for false discovery rate (FDR). Methylation and expression data were tested for correlation.

We selected a subgroup of 24 samples among the 192 initial samples, including 12 normoglycemic and 12 T2D cases, to analyze DNA methylation in blood samples from the same donors. The 24 samples were selected based on their expression and methylation profiles using PCA to reduce the heterogeneity.

Materials. The PDGFRα inhibitor Ki11502, human PDGF-AA recombinant, Phorbol 12-Myristate 13-myristate (PMA), Metformin and Wortmaninn were purchased from Sigma-Aldrich. The anti-PDGF-AA blocking antibodies were from Merckmillipore. The PKC inhibitor Sautrostaurin was from Selleckchem.

Cell Culture. Immortalized Human Hepatocytes (IHH) [53] were cultured in Williams E medium (Invitrogen), containing 11 mM glucose and supplemented with 10 % fetal calf serum (FCS; Eurobio), 100 U/ml penicillin, 100 µg/ml streptomycin, 20 mU/ml insulin (Sigma-Aldrich) and 50 nM dexamethasone (Sigma-Aldrich). For insulin pre-treatment, 10^6 cells were cultured in 6-well plates in a Dulbecco's Modified Eagle Medium (DMEM; Invitrogen) with or without 100 nM human insulin (Novo Nordisk) supplemented with 5 mM Glucose, 2 % FCS, 100 U/ml penicillin, 100 µg/ml streptomycin for 24 hours. For monitoring insulin signaling, medium was removed and replaced by FCS- and phenol red-free DMEM medium with or without 200 nM human insulin for one hour. Human hepatocytes were isolated from liver lobectomies resected for medical reasons as described [54] in agreement with the ethics procedures and adequate authorization.

Quantitative PCR. Total RNA was extracted from IHH cells according to the manufacturer's protocol (RNeasy Lipid Tissue Kit, Qiagen). The RNA purity and concentration were determined by RNA Integrity Number (RNA 6000 Nano Kit, 2100 Bioanalyser, Agilent). Total RNA was transcribed into cDNA as described [55]. Each cDNA sample was quantified by quantitative real-time polymerase chain reaction using the fluorescent TaqMan 5′-nuclease assays or a BioRad MyiQ Single-Color Real-Time PCR Detection System using the BioRad iQ SYBR Green Supermix, with 100 nM primers and 1 µl of template per 20 µl of PCR and an

annealing temperature of 60 °C. Gene expression analysis was normalized against Beta-Glucuronidase (*GUSB*) expression or 60S acidic ribosomal protein P0 (*RPLP0*). The primer sequences are available in the supplemental information.

Western Blotting and ELISA. Cells were scrapped in cold PBS buffer and then cells pellet was incubated for 30 minutes on ice in the following lysis buffer (20 mM Tris acetate pH 7, 0.27 mM Sucrose, 1% Triton X-100, 1 mM EDTA, 1 mM EGTA, 1 mM DTT) supplemented with antiproteases and antiphosphatases (Roche, Meylan, France). Cell lysate was centrifuged 15 minutes at 18,000g and supernatant was collected as total proteins. For Western blotting experiments, 40 µg of total protein extract was separated on 10% SDS-Polyacrylamide gel and electrically blotted to nitrocellulose membrane. The proteins were detected after an overnight incubation of the membrane at 4°C with the specific primary antibodies against AKT (Santa Cruz Biotechnology, dilution 1:1000), PKCϴ (Abcam, dilution 1:1000), PKCε (Abcam, dilution 1:1000), IRS1 (Cell Signaling Biotechnology, dilution 1:1000), PDGF-AA (Merck Millipore, dilution 1:1000), αtubulin (Sigma, dilution 1:5000), phospho-AKT (Ser-473; Cell Signaling Biotechnology, dilution 1:1000), phospho-PKCϴ (Ser-676, Abcam, dilution 1:1000), phospho-PKCε (Ser-729, Abcam, dilution 1:1000) in buffer containing 0.1% Tween 20 with either five percent BSA or five milk (for αtubulin). Proteins were visualized with IRDye800 or IRDye700 (Eurobio) as secondary antibodies. Quantification was performed using the Odyssey Infrared Imaging System (Eurobio). PDGFA released in the cell supernatant was quantified by ELISA kit (R &D Systems) according to the manufacturer's protocol.

RNA sequencing, Glycogen measurement, Global Serine/Threonine kinases activity, DNA/RNA preparation, Oil-Red staining, cell proliferation, apoptosis, intermediate

metabolic traits. See the supplemental experimental procedure in the supplemental information

Author contributions

PF, SC, LY and AA designed the study. LY, AA, MC, AB and PF drafted and wrote the manuscript. LY and MC performed statistical analyses. AB, OS and IR performed the bioinformatics analysis. SL, JM, JD, GL, LR, MK, MT, JB, EA, SS, PJ, RB, SGC, VP, AL and MDC performed the experiments. AA, SC, MC, RC, VR, SL, JM, LR, GL, AL, TD, PM, BS, AS, JA, CP, JH, AB, FP and PF revised the manuscript. All authors have read and approved the final version of the manuscript.

Acknowledgements

This study was supported by nonprofit organizations and public bodies for funding of scientific research conducted in France and within the European Union: "*Centre National de la Recherche Scientifique*", "*Université de Lille 2*", "*Institut Pasteur de Lille*", "*Société Francophone du Diabète*", "*Contrat de Plan Etat-Région*", "*Agence Nationale de la Recherche*", ANR-10-LABX-46, ANR EQUIPEX Ligan MP : ANR-10-EQPX-07-01, European Research Council GEPIDIAB - 294785. We are grateful to Ms Estelle Leborgne for helping in the illustrations of the manuscript.

References

1. Bonnefond, A. & Froguel, P. Rare and common genetic events in type 2 diabetes: what should biologists know? *Cell Metab.* **21,** 357–368 (2015).
2. Stefan, N. & Häring, H.-U. The Metabolically Benign and Malignant Fatty Liver. *Diabetes* **60,** 2011–2017 (2011).
3. Ling, C. & Groop, L. Epigenetics: A Molecular Link Between Environmental Factors and Type 2 Diabetes. *Diabetes* **58,** 2718–2725 (2009).
4. Kirchner, H. *et al.* Altered DNA methylation of glycolytic and lipogenic genes in liver from obese and type 2 diabetic patients. *Mol. Metab.* **5,** 171–183 (2016).
5. Muka, T. *et al.* The role of global and regional DNA methylation and histone modifications in glycemic traits and type 2 diabetes: A systematic review. *Nutr. Metab. Cardiovasc. Dis. NMCD* (2016). doi:10.1016/j.numecd.2016.04.002
6. Nilsson, E. *et al.* Altered DNA Methylation and Differential Expression of Genes Influencing Metabolism and Inflammation in Adipose Tissue From Subjects With Type 2 Diabetes. *Diabetes* **63,** 2962–2976 (2014).
7. Wahl, S. *et al.* Epigenome-wide association study of body mass index, and the adverse outcomes of adiposity. *Nature* **541,** 81–86 (2017).
8. Houseman, E. A. *et al.* Reference-free deconvolution of DNA methylation data and mediation by cell composition effects. *BMC Bioinformatics* **17,** 259 (2016).
9. Ahrens, M. *et al.* DNA methylation analysis in nonalcoholic fatty liver disease suggests distinct disease-specific and remodeling signatures after bariatric surgery. *Cell Metab.* **18,** 296–302 (2013).
10. Kirchner, H. *et al.* Altered DNA methylation of glycolytic and lipogenic genes in liver from obese and type 2 diabetic patients. *Mol. Metab.* **5,** 171–183 (2016).

11. Murphy, S. K. *et al.* Relationship between methylome and transcriptome in patients with nonalcoholic fatty liver disease. *Gastroenterology* **145,** 1076–1087 (2013).
12. Zeybel, M. *et al.* Differential DNA methylation of genes involved in fibrosis progression in non-alcoholic fatty liver disease and alcoholic liver disease. *Clin. Epigenetics* **7,** 25 (2015).
13. Hayes, B. J. *et al.* Activation of Platelet-Derived Growth Factor Receptor Alpha Contributes to Liver Fibrosis. *PLoS ONE* **9,** (2014).
14. Kocabayoglu, P. *et al.* β-PDGF receptor expressed by hepatic stellate cells regulates fibrosis in murine liver injury, but not carcinogenesis. *J. Hepatol.* **63,** 141–147 (2015).
15. Liu, X. & Brenner, D. A. Liver: DNA methylation controls liver fibrogenesis. *Nat. Rev. Gastroenterol. Hepatol.* **13,** 126–128 (2016).
16. Thieringer, F. *et al.* Spontaneous hepatic fibrosis in transgenic mice overexpressing PDGF-A. *Gene* **423,** 23–28 (2008).
17. Scott, R. A. *et al.* Large-scale association analyses identify new loci influencing glycemic traits and provide insight into the underlying biological pathways. *Nat Genet* **44,** 991–1005 (2012).
18. Wong, N. C. *et al.* Exploring the utility of human DNA methylation arrays for profiling mouse genomic DNA. *Genomics* **102,** 38–46 (2013).
19. Marra, F., Choudhury, G. G., Pinzani, M. & Abboud, H. E. Regulation of platelet-derived growth factor secretion and gene expression in human liver fat-storing cells. *Gastroenterology* **107,** 1110–1117 (1994).
20. Baumeier, C. *et al.* Hepatic DPP4 DNA Methylation Associates With Fatty Liver. *Diabetes* **66,** 25–35 (2017).

21. Lubura, M. *et al.* Diabetes prevalence in NZO females depends on estrogen action on liver fat content. *Am. J. Physiol. - Endocrinol. Metab.* ajpendo.00338.2015 (2015). doi:10.1152/ajpendo.00338.2015
22. Mackenzie, R. W. & Elliott, B. T. Akt/PKB activation and insulin signaling: a novel insulin signaling pathway in the treatment of type 2 diabetes. *Diabetes Metab. Syndr. Obes. Targets Ther.* **7,** 55–64 (2014).
23. Nishioka, C. *et al.* Ki11502, a novel multitargeted receptor tyrosine kinase inhibitor, induces growth arrest and apoptosis of human leukemia cells in vitro and in vivo. *Blood* **111,** 5086–5092 (2008).
24. Hilhorst, R. *et al.* in *Gene Regulation* (ed. Bina, M.) **977,** 259–271 (Humana Press, 2013).
25. Dasgupta, S. *et al.* Mechanism of lipid induced insulin resistance: Activated PKCε is a key regulator. *Biochim. Biophys. Acta BBA - Mol. Basis Dis.* **1812,** 495–506 (2011).
26. Kim, J. K. *et al.* PKC-θ knockout mice are protected from fat-induced insulin resistance. *J. Clin. Invest.* **114,** 823–827 (2004).
27. Samuel, V. T. *et al.* Inhibition of protein kinase Cε prevents hepatic insulin resistance in nonalcoholic fatty liver disease. *J. Clin. Invest.* **117,** 739–745 (2007).
28. Cenni, V. *et al.* Regulation of novel protein kinase C ε by phosphorylation. *Biochem. J.* **363,** 537–545 (2002).
29. Liu, Y., Graham, C., Li, A., Fisher, R. J. & Shaw, S. Phosphorylation of the protein kinase C-theta activation loop and hydrophobic motif regulates its kinase activity, but only activation loop phosphorylation is critical to in vivo nuclear-factor-κB induction. *Biochem. J.* **361,** 255–265 (2002).
30. Evenou, J.-P. *et al.* The Potent Protein Kinase C-Selective Inhibitor AEB071 (Sotrastaurin) Represents a New Class of Immunosuppressive Agents Affecting Early T-Cell Activation. *J. Pharmacol. Exp. Ther.* **330,** 792–801 (2009).

31. Rodr&#xed *et al.* Metformin Induces Cell Cycle Arrest and Apoptosis in Drug-Resistant Leukemia Cells. *Leuk. Res. Treat.* **2015,** e516460 (2015).
32. Anstee, Q. M. & Day, C. P. The genetics of NAFLD. *Nat. Rev. Gastroenterol. Hepatol.* **10,** 645–655 (2013).
33. Cofer, Z. C. *et al.* Methylation Microarray Studies Highlight PDGFA Expression as a Factor in Biliary Atresia. *PLOS ONE* **11,** e0151521 (2016).
34. Boonjaraspinyo, S. *et al.* Platelet-derived growth factor may be a potential diagnostic and prognostic marker for cholangiocarcinoma. *Tumour Biol. J. Int. Soc. Oncodevelopmental Biol. Med.* **33,** 1785–1802 (2012).
35. Michelini, E. *et al.* Is cholangiocarcinoma another complication of insulin resistance: a report of three cases. *Metab. Syndr. Relat. Disord.* **5,** 194–202 (2007).
36. Andrae, J., Gallini, R. & Betsholtz, C. Role of platelet-derived growth factors in physiology and medicine. *Genes Dev.* **22,** 1276–1312 (2008).
37. Awuah, P. K., Nejak-Bowen, K. N. & Monga, S. P. S. Role and Regulation of PDGFRα Signaling in Liver Development and Regeneration. *Am. J. Pathol.* **182,** 1648–1658 (2013).
38. Thieringer, F. *et al.* Spontaneous hepatic fibrosis in transgenic mice overexpressing PDGF-A. *Gene* **423,** 23–28 (2008).
39. Kikuchi, A. & Monga, S. P. PDGFRα in liver pathophysiology: emerging roles in development, regeneration, fibrosis, and cancer. *Gene Expr.* **16,** 109–127 (2015).
40. Bril, F. *et al.* Relationship between disease severity, hyperinsulinemia, and impaired insulin clearance in patients with nonalcoholic steatohepatitis. *Hepatology* **59,** 2178–2187 (2014).
41. Zick, Y. Ser/Thr Phosphorylation of IRS Proteins: A Molecular Basis for Insulin Resistance. *Sci STKE* **2005,** pe4-pe4 (2005).
42. Dyson, J. K., Anstee, Q. M. & McPherson, S. Republished: Non-alcoholic fatty liver disease: a practical approach to treatment. *Postgrad. Med. J.* **91,** 92–101 (2015).

43. Bo, S., Benso, A., Durazzo, M. & Ghigo, E. Does use of metformin protect against cancer in Type 2 diabetes mellitus? *J. Endocrinol. Invest.* **35,** 231–235 (2012).

44. Hägerkvist, R., Jansson, L. & Welsh, N. Imatinib mesylate improves insulin sensitivity and glucose disposal rates in rats fed a high-fat diet. *Clin. Sci.* **114,** 65–71 (2008).

45. Breccia, M., Muscaritoli, M., Aversa, Z., Mandelli, F. & Alimena, G. Imatinib Mesylate May Improve Fasting Blood Glucose in Diabetic Ph+ Chronic Myelogenous Leukemia Patients Responsive to Treatment. *J. Clin. Oncol.* **22,** 4653–4655 (2004).

46. Veneri, D., Franchini, M. & Bonora, E. Imatinib and regression of type 2 diabetes. *N. Engl. J. Med.* **352,** 1049–1050 (2005).

47. Caiazzo, R. *et al.* Roux-en-Y gastric bypass versus adjustable gastric banding to reduce nonalcoholic fatty liver disease: a 5-year controlled longitudinal study. *Ann. Surg.* **260,** 893-898-899 (2014).

48. Bibikova, M. *et al.* High density DNA methylation array with single CpG site resolution. *Genomics* **98,** 288–295 (2011).

49. Voight, B. F. *et al.* The metabochip, a custom genotyping array for genetic studies of metabolic, cardiovascular, and anthropometric traits. *PLoS Genet.* **8,** e1002793 (2012).

50. Team, R. C. *R: A language and environment for statistical computing. R Foundation for Statistical Computing, Vienna, Austria, 2012*. (ISBN 3-900051-07-0, 2014).

51. Aryee, M. J. *et al.* Minfi: a flexible and comprehensive Bioconductor package for the analysis of Infinium DNA methylation microarrays. *Bioinforma. Oxf. Engl.* **30,** 1363–1369 (2014).

52. Teschendorff, A. E. *et al.* A beta-mixture quantile normalization method for correcting probe design bias in Illumina Infinium 450 k DNA methylation data. *Bioinforma. Oxf. Engl.* **29,** 189–196 (2013).

53. Samanez, C. H. *et al.* The human hepatocyte cell lines IHH and HepaRG: models to study glucose, lipid and lipoprotein metabolism. *Arch. Physiol. Biochem.* **118,** 102–111 (2012).
54. Pichard, L. *et al.* Human hepatocyte culture. *Methods Mol. Biol. Clifton NJ* **320,** 283–293 (2006).
55. Bonner, C. *et al.* Inhibition of the glucose transporter SGLT2 with dapagliflozin in pancreatic alpha cells triggers glucagon secretion. *Nat. Med.* (2015). doi:10.1038/nm.3828

Legends of Figures

Fig. 1. a) Quantile-quantile (qq-) plot showing the residual inflation of test statistics before and after genomic-control correction. **b**) Manhattan plot centered on *PDGFA* cg14496282 methylation site showing association signal within *PDGFA* bounds.

Fig. 2. a) PDGF-AA secretion from IHH cells and primary human hepatocytes was measured by ELISA kit. **b**) and **c**) Increase of *PDGFA* mRNA by insulin. IHH cells were cultured with 100 nM human insulin (NovoNordisk) for the indicated times. The *PDGFA* mRNA level was quantified by qRT-PCR and normalized against *GUSB.* The expression levels from untreated cells were set to 100 %. Data are the mean ± SEM (*: $p < 0.05$). **d**) Methylation levels at *PDGFA* cg14496282 in response to insulin. IHH cells were cultured in a culture medium containing 5 mM Glucose, 2 % FCS with or without 100 nM human insulin for 24 hrs. Methylation level at the cg14496282 was quantified by the Infinium HumanMethylation450 BeadChip. **e**) *PDGFA* mRNA level in mice liver in response to insulin. Insulin (I.P. 5U/Kg) or vehicle was injected for 10 minutes in overnight fasted C57Bl/6 mice males (n=5/groups). **f)** PDGF-AA abundance in IHH cells cultured with insulin. IHH cells were cultured with 100 nM human insulin for the indicated times. PDGF-AA content was quantified by Western Blotting experiments. The blot is one representative out of three independent experiments. Effect of wortmannin on **g**) the *PDGFA* mRNA by qRT-PCR and **h**) PDGF-AA protein levels by Western Blotting experiments. IHH cells were co-cultured with 100 nM human insulin in the presence of vehicle or 1 μM wortmannin for the indicated times or 24 hrs.

Fig. 3. Hepatic *Pdgfa* expression in **a**-**b**) 6 weeks old male B6 mice and in **c**-**d**) 10 weeks old diabetes-prone female New Zealand Obese (NZO) mice . **a**) and **c**) show results of array data;

b) and **d**) those of qRT-PCR. Differences between DIO-responder (Resp, black circle) and DIO-non-responder (nResp, white circle) mice as well as between diabetes-prone (DP, black squares) and diabetes-resistant (DR, white squares) were calculated by Student's t test. * P<0.05, ** P<0.01, *** P<0.001. **e**) PDGFA mRNA level in BXD mice fed on a HFD fed for 21 weeks. * indicates p value < 0.0001 by unpaired t test with Welch's correction.

Fig. 4. a) PDGF-AA secretion in response to insulin. IHH cells were cultured with insulin for the indicated times. The measurement of PDGF-AA from the supernatant was achieved by ELISA. **b**) Measurement of insulin-induced AKT phosphorylation in response to insulin pre-treatment. IHH cells were incubated in a culture medium containing 5 mM Glucose, 2 % FCS with or without 100 nM human insulin for the indicated times. AKT phosphorylation was stimulated by insulin for one hour. Immunoblotting for phospho-AKT (P-AKT) was done using the anti phospho-AKT (Serine 473) antibodies. The Fig. shows the result of a representative experiment out of three. **c**) Effect of insulin treatment on glycogen deposition. IHH cells were cultured with insulin for the indicated times. Thereafter, glycogen was monitored after stimulating cells in a KRP buffer without (Ctrl) or with insulin for 1 hr and 20 mM glucose. Glycogen was monitored by ELISA. Effects of insulin on the expression of **d**) *IRS1* mRNA by qRT-PCR and **e**) IRS1 protein content by Western Blotting experiments in IHH cells cultured with insulin for the indicated times. Effects of **f**) PDGF-AA, **g**) PDGFA blocking antibodies or **h**) the PDGFR inhibitor ki11502 on insulin-induced AKT activation. For **f**) activation of AKT was monitored by western blotting using total proteins from IHH cells that were cultured with the human recombinant PDGF-AA at the indicated concentrations for 24 hrs, which subsequently were incubated with 200 nM insulin for stimulating AKT phosphorylation. For **f-h**, IHH cells were co-incubated in a culture medium containing 5 mM Glucose, 2 % FCS with or without 100 nM human insulin for 24 hours plus **f**) PDGF-AA at the indicated concentration,

g) PDGFA antibodies (+; 0.75 μg or ++; 1.5 μg) or **h**) ki11502 at the indicated concentration. The Figures show the result of a representative experiment out of three. **i**) Effect of the PDGFR inhibitor ki11502 on the glycogen production. Glycogen was measured by ELISA in IHH cells that were co-cultured with 5 μM ki11502 and insulin for the indicated times. **j**) Volcano plot showing differences in putative serine/threonine kinase activities between control and insulin-treated IHH cells for 24 hrs. Specific and positive kinase statistic (in red) show higher activity in IHH cultured with insulin compared with control samples. Effects of **k**) insulin and **l**) PDGF-AA on the phosphorylation of PKCΘ and PKCε. IHH cells were cultured with insulin for the indicated times or PDGF-AA (for 24 hrs). Phosphorylation of PKCΘ (Ser 676) and PKCε (Ser 729) were measured by western blotting and normalized against total PKCΘ and PKCε. **m**) Effect of PDGF-AA on the IRS1 protein content. IHH cells were cultured for 24 hrs with PDGF-AA at the indicated concentrations. Effect of **n**) PDGF-AA and **o**) insulin on the expression of *PDGFA*. The *PDGFA* mRNA level was quantified by qRT-PCR in IHH cells co-cultured with either 100 ng/ml PDGF-AA for 24 hrs or insulin with or without the PDGFR inhibitor Ki11502 for the indicated times. Effect of **p**) PKC activator phorbol 12-myristate 13-acetate (PMA) or the PKC inhibitor sotraustorin on the expression of *PDGFA* mRNA either **q**) induced by insulin for the indicated times or **r**) by PDGF-AA. *PDGFA* mRNA was quantified in IHH cells cultured with either PMA for the indicated times or 100 ng/ml PDGF-AA in the presence or absence of 1 μM sotrastaurin for 24 hrs. Effect of metformin on the **s**) PDGFA mRNA level and PDGF-AA **t**) intracellular abundance and **u**) secretion induced by 100 nM insulin for the indicated times.

Fig. 5: Schematic representation of the mechanism linking chronic hyperinsulinemia to hepatic insulin resistance in T2D. Insulin promotes hypomethylation and the rise of *PDGFA* expression,

leading to PDGF-AA secretion. In turn, PDGF-AA inhibits the insulin signaling, in a negative autocrine feedback loop, via a mechanism involving a decrease in the IRS1 abundance and PKC (PKCϴ and PKCε) activation.

Tables

Table 1. Association of liver methylation levels of cg14496282 and liver *PDGFA* gene expression with multiple quantitative and binary traits. Methylation levels at cg14496282 and *PDGFA* gene expression are the endogenous variable in all linear regressions used to measure associations. SD: Standard Deviation.

Traits(unit)	***PDGFA* cg14496282 methylation**		***PDGFA* Expression**	
	Effect size in % of methylation / trait unit (*p*-value)		**Effect size in SD/trait unit (*p*-value)**	
	Controls	**T2D cases**	**Controls**	**T2D cases**
cg14496282 methylation (%)			**-1.44 (6.27×10^{-3})**	**-2.49 (4.94×10^{-3})**
PDGFA expression (SD)	**-0.05 (6.27×10^{-3})**	**-0.03 (4.94×10^{-3})**		
Fasting glucose (mmol/l)	-0.01 (0.79)	-	0.29 (0.196)	-
Fasting insulin (pmol/l)	**-1.45×10^{-3} (2.32×10^{-3})**	-	**6.83×10^{-3} (9.49×10^{-3})**	-
HOMA2-B (unitless - log)	**-0.17 (2.92×10^{-3})**	-	**0.63 (0.038)**	-
HOMA2-IR (unitless - log)	**-0.10 (4.93×10^{-3})**	-	**0.53 (7.47×10^{-3})**	-
QUICKI (unitless)	**1.66 (0.01)**	-	**-9.19 (9.78×10^{-3})**	-
Steatosis (%)	**-2.15×10^{-3} (0.01)**	-4.34×10^{-4} (0.42)	**0.01 (2.72×10^{-3})**	**0.02 (2.14×10^{-6})**
NASH (Yes/ No)	**-0.17 (0.04)**	**-0.072 (0.03)**	**2.11 (9.38×10^{-7})**	**1.45 (3.37×10^{-8})**
Hepatic fibrosis (Yes/ No)	-0.07 (0.09)	**-0.051 (0.04)**	0.19 (0.434)	**0.63 (2.66×10^{-3})**
Alanine aminotransferase (UI/L)	-1.44×10^{-4} (0.89)	**-1.34×10^{-3} (0.03)**	0.01 (0.067)	**0.02 (1.46×10^{-4})**
Aspartate aminotransferase (UI/L)	-4.71×10^{-3} (0.06)	**-1.76×10^{-3} (0.04)**	**0.03 (7.89×10^{-3})**	**0.03 (2.56×10^{-6})**

Fig. 1

a

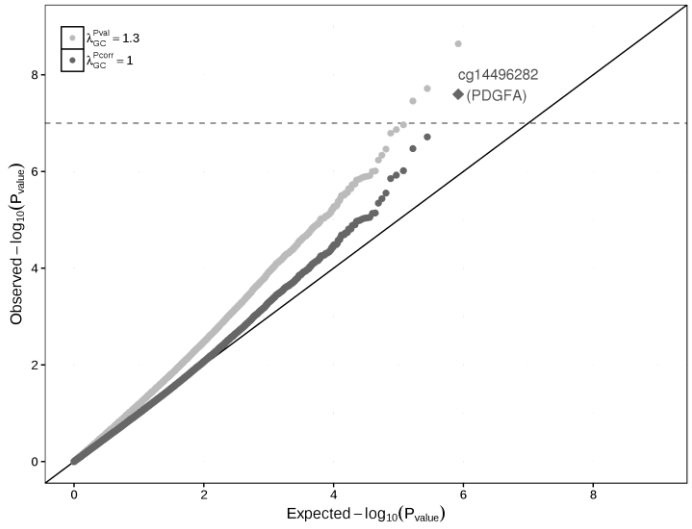
$\lambda_{GC}^{Pval} = 1.3$
$\lambda_{GC}^{Pcorr} = 1$
cg14496282
(PDGFA)
Observed – $\log_{10}(P_{value})$
Expected – $\log_{10}(P_{value})$
0
2
4
6
8

b

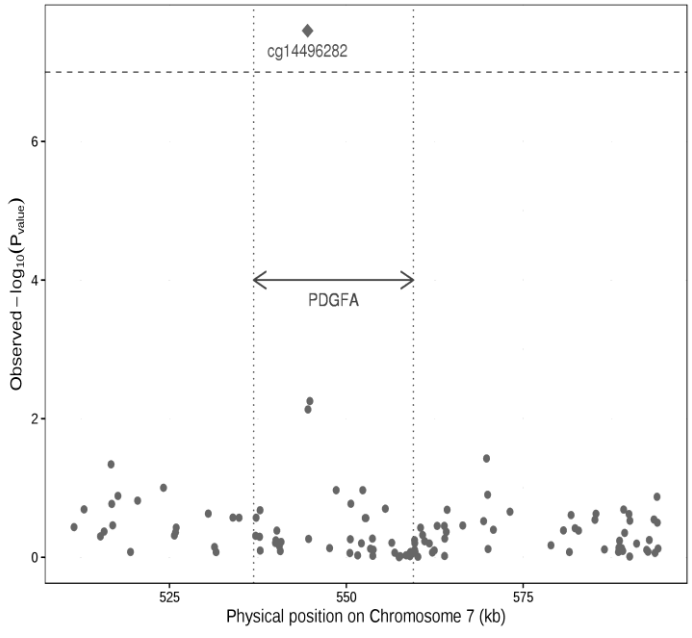
cg14496282
PDGFA
Observed – $\log_{10}(P_{value})$
Physical position on Chromosome 7 (kb)
0
2
4
6
525
550
575

Fig. 2

a

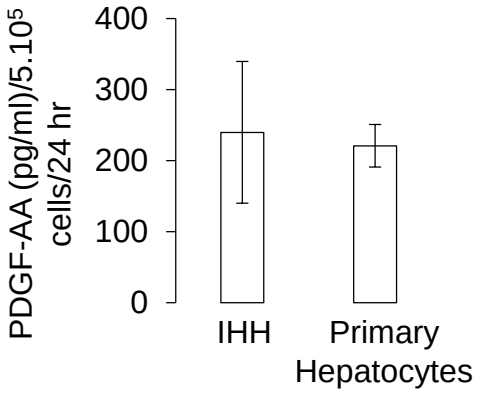
PDGF-AA (pg/ml)/5.10^5 cells/24 hr
400
300
200
100
0
IHH
Primary Hepatocytes

b

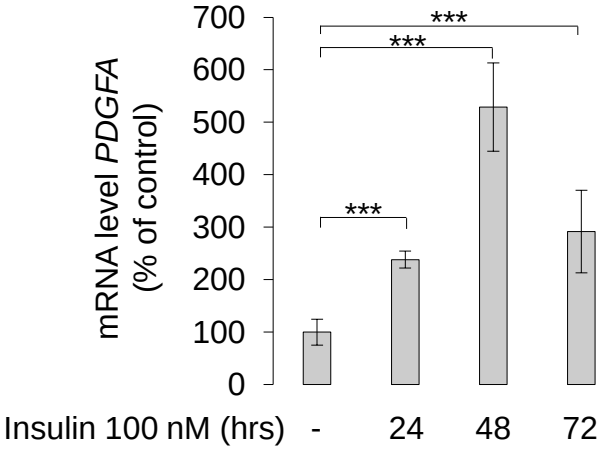
mRNA level *PDGFA* (% of control)
700
600
500
400
300
200
100
0
***
***
***
Insulin 100 nM (hrs)
-
24
48
72

c

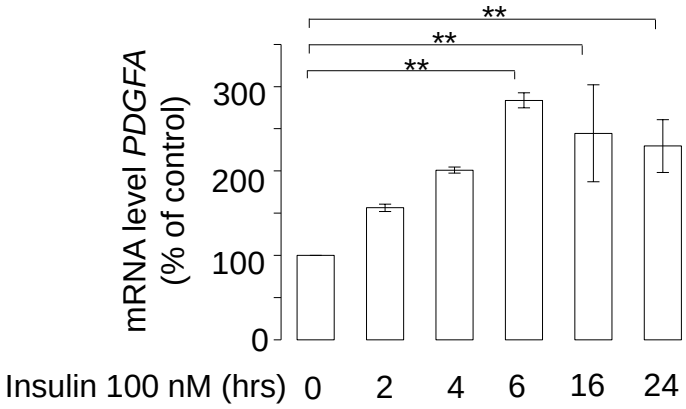
mRNA level *PDGFA* (% of control)
300
200
100
0
**
**
**
Insulin 100 nM (hrs)
0
2
4
6
16
24

d

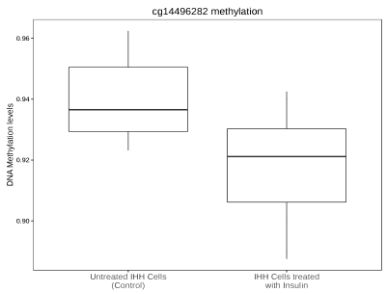
cg14496282 methylation
DNA Methylation levels
0.96
0.94
0.92
0.90
Untreated IHH Cells (Control)
IHH Cells treated with Insulin

Fig. 2

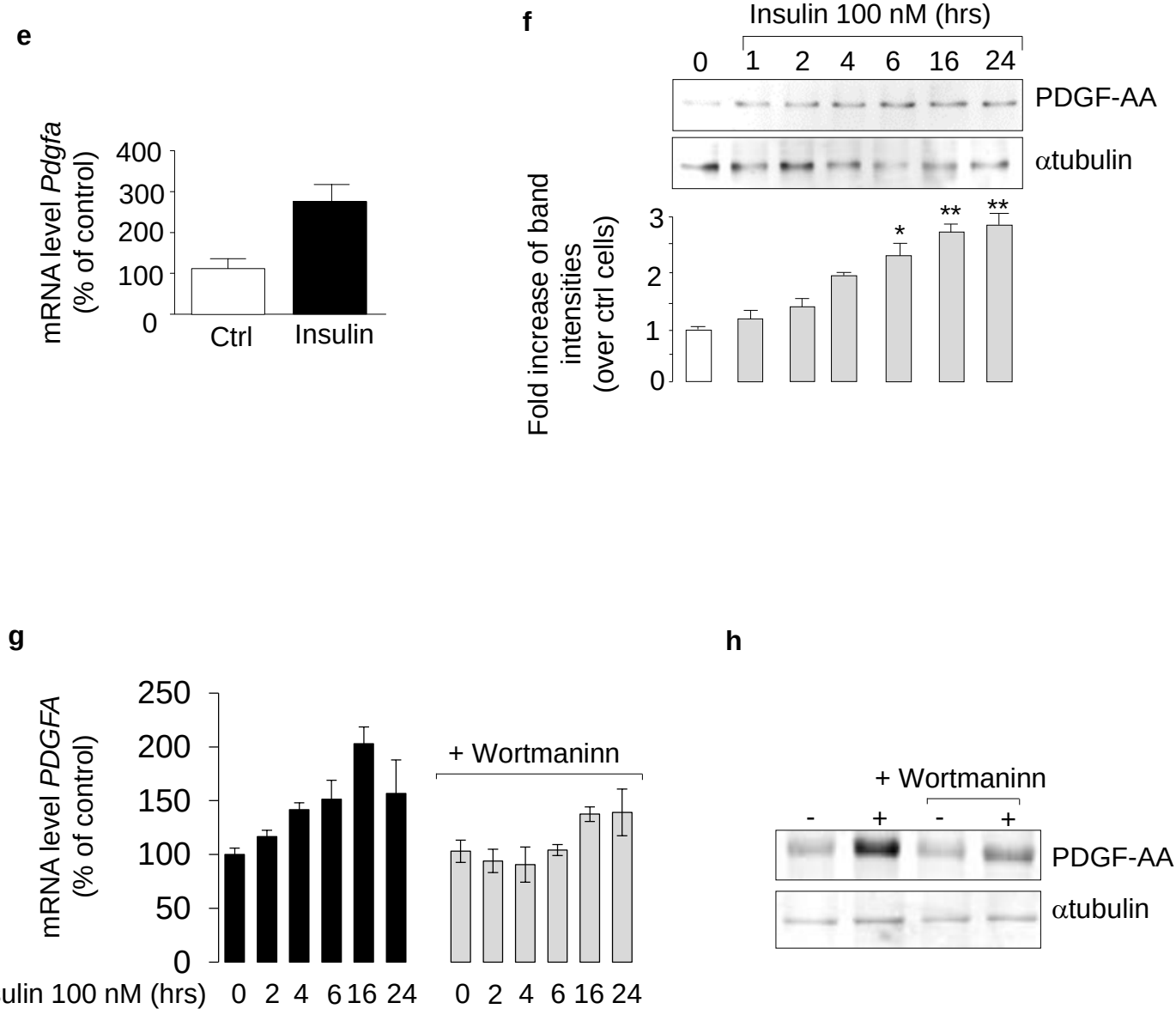
e
mRNA level Pdgfa (% of control)
400
300
200
100
0
Ctrl
Insulin
f
Insulin 100 nM (hrs)
0 1 2 4 6 16 24
PDGF-AA
αtubulin
Fold increase of band intensities (over ctrl cells)
3
2
1
0
*
**
**
g
mRNA level PDGFA (% of control)
250
200
150
100
50
0
+ Wortmaninn
Insulin 100 nM (hrs) 0 2 4 6 16 24 0 2 4 6 16 24
h
+ Wortmaninn
- + - +
PDGF-AA
αtubulin

Fig. 3

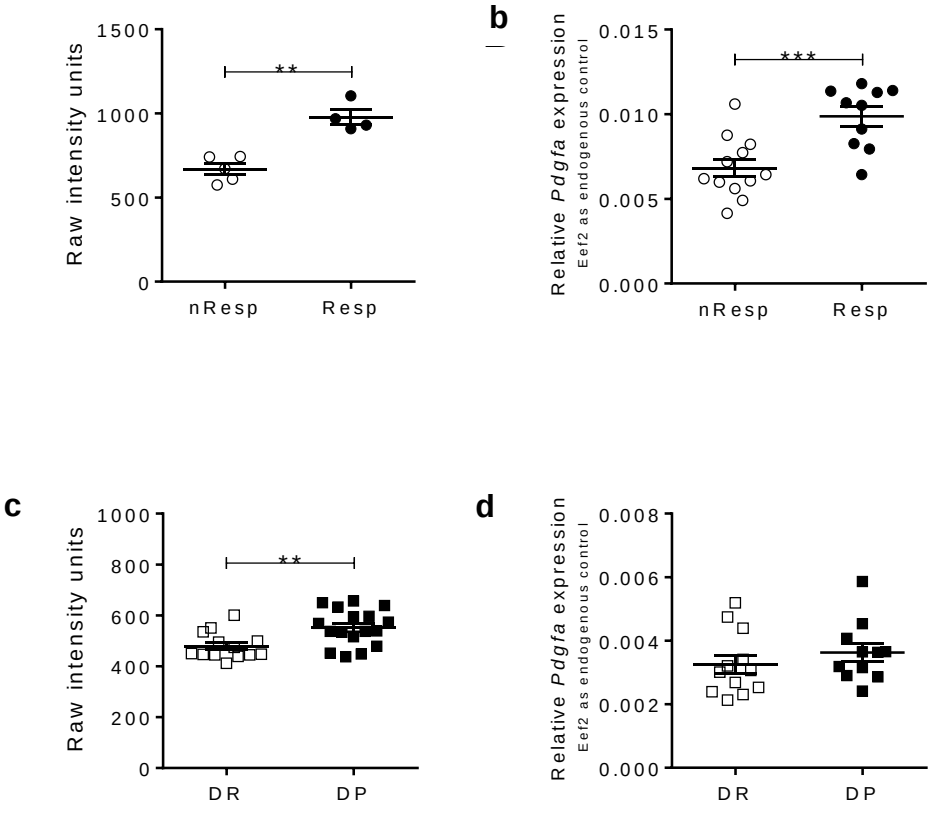
b
Raw intensity units
1500
1000
500
0
**
nResp
Resp
Relative Pdgfa expression
Eef2 as endogenous control
0.015
0.010
0.005
0.000
***
nResp
Resp
c
Raw intensity units
1000
800
600
400
200
0
**
DR
DP
d
Relative Pdgfa expression
Eef2 as endogenous control
0.008
0.006
0.004
0.002
0.000
DR
DP

Fig. 3e

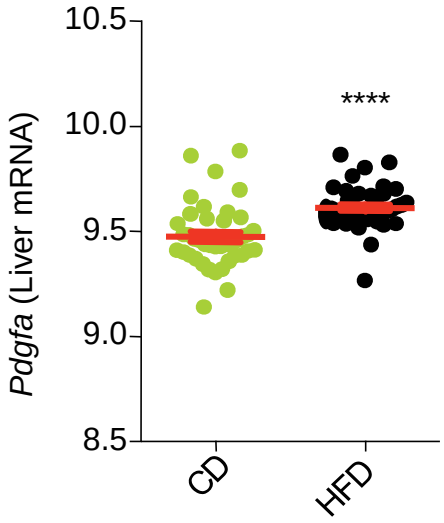

Fig. 4a

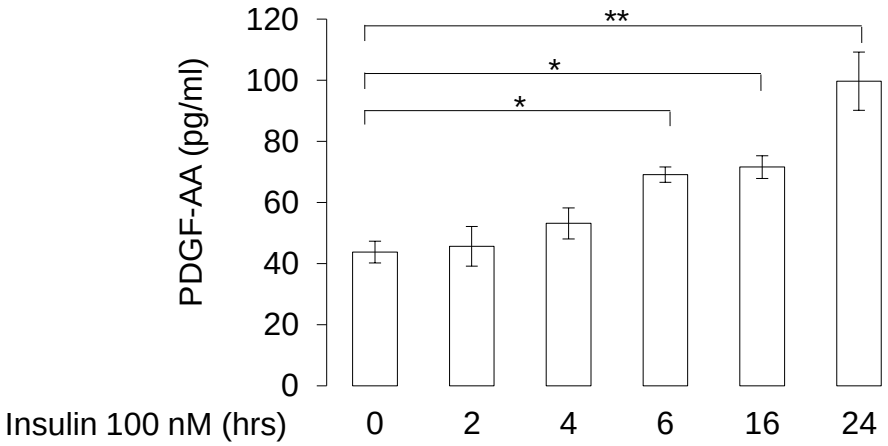

Fig. 4

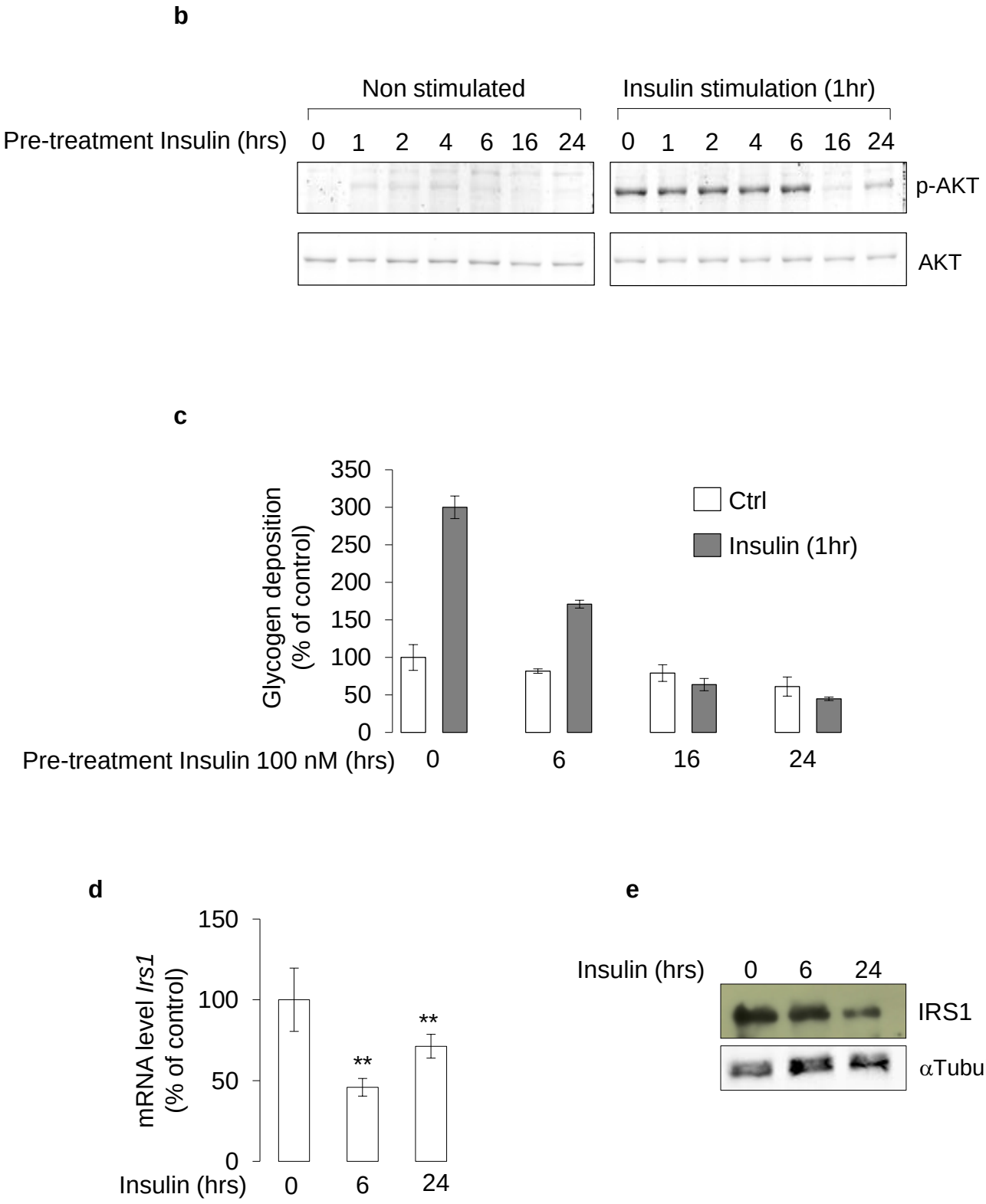
b
Non stimulated
Insulin stimulation (1hr)
Pre-treatment Insulin (hrs)
0 1 2 4 6 16 24
0 1 2 4 6 16 24
p-AKT
AKT
c
Glycogen deposition (% of control)
350
300
250
200
150
100
50
0
Ctrl
Insulin (1hr)
Pre-treatment Insulin 100 nM (hrs)
0
6
16
24
d
mRNA level Irs1 (% of control)
150
100
50
0
**
**
Insulin (hrs)
0
6
24
e
Insulin (hrs)
0 6 24
IRS1
αTubulin

Fig. 4

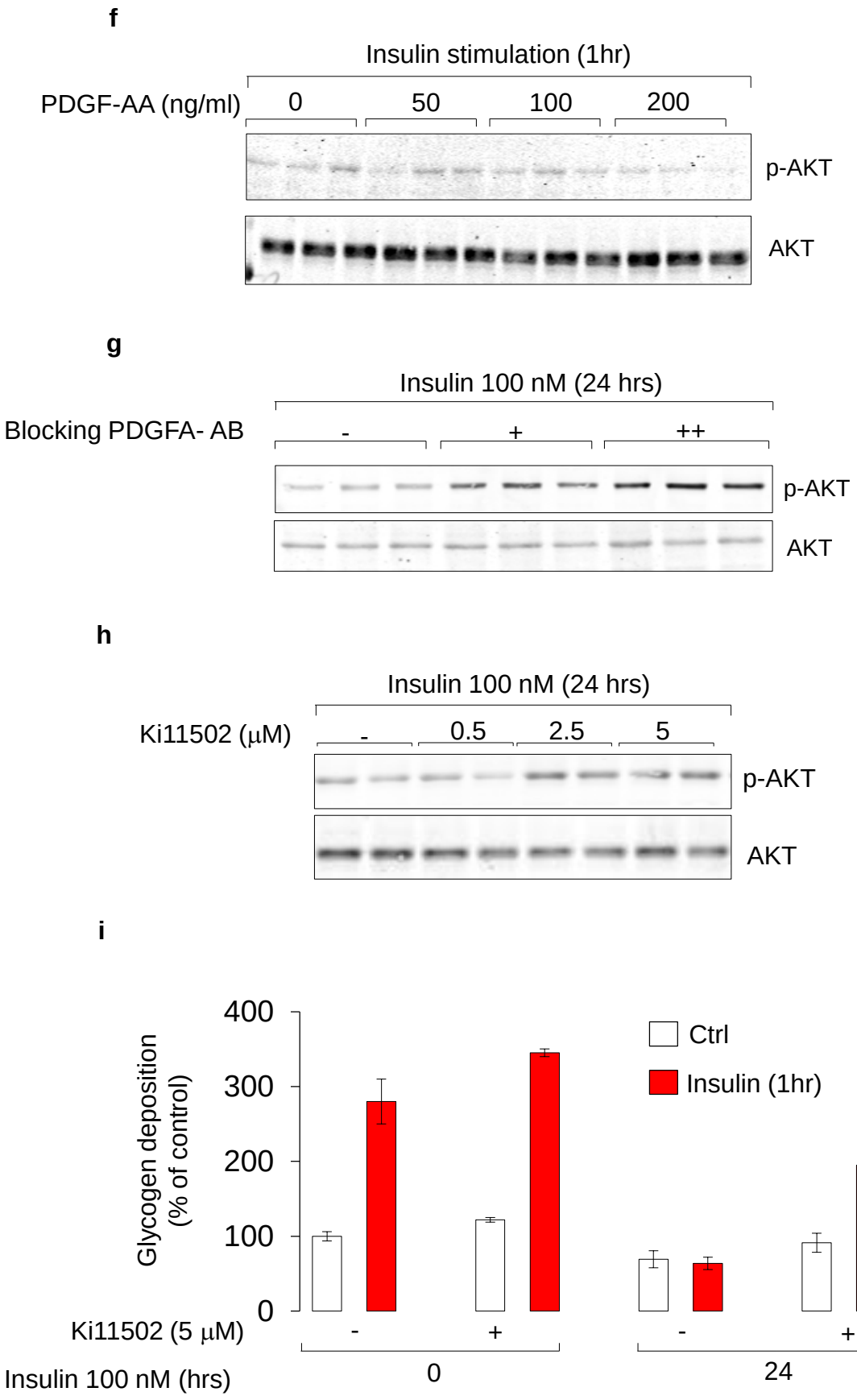
f
Insulin stimulation (1hr)
PDGF-AA (ng/ml)
0
50
100
200
p-AKT
AKT
g
Insulin 100 nM (24 hrs)
Blocking PDGFA- AB
-
+
++
p-AKT
AKT
h
Insulin 100 nM (24 hrs)
Ki11502 (μM)
-
0.5
2.5
5
p-AKT
AKT
i
Glycogen deposition (% of control)
400
300
200
100
0
Ctrl
Insulin (1hr)
Ki11502 (5 μM)
-
+
-
+
Insulin 100 nM (hrs)
0
24

Fig. 4

j

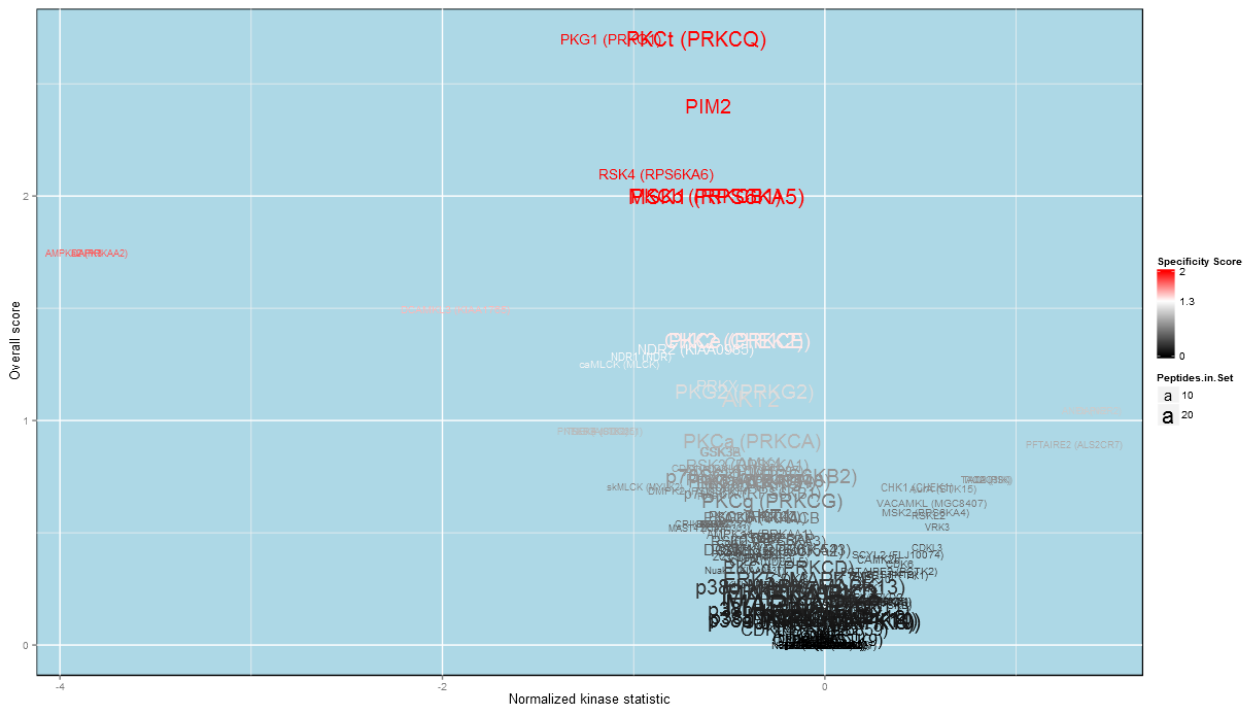
PKG1 (PRKG1)
PKCt (PRKCQ)
PIM2
RSK4 (RPS6KA6)
PKG2 (PRKG2)
PKCa (PRKCA)
PKCg (PRKCG)
PKCd (PRKCD)
PFTAIRE2 (ALS2CR7)
VACAMKL (MGC8407)
Overall score
Normalized kinase statistic
Specificity Score
Peptides.in.Set

k

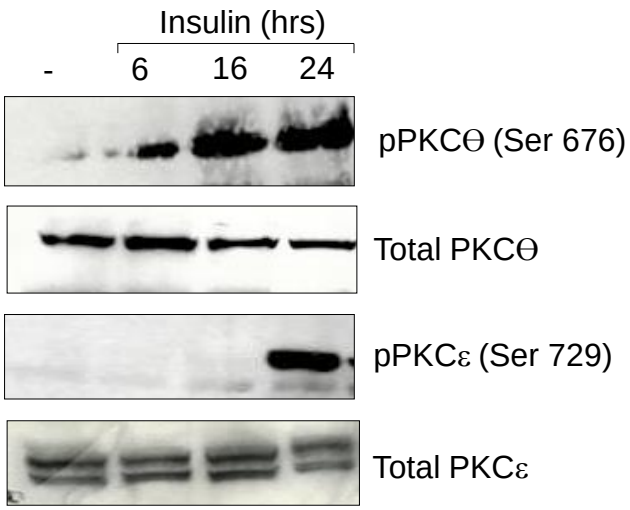
Insulin (hrs)
-
6
16
24
pPKCΘ (Ser 676)
Total PKCΘ
pPKCε (Ser 729)
Total PKCε

l

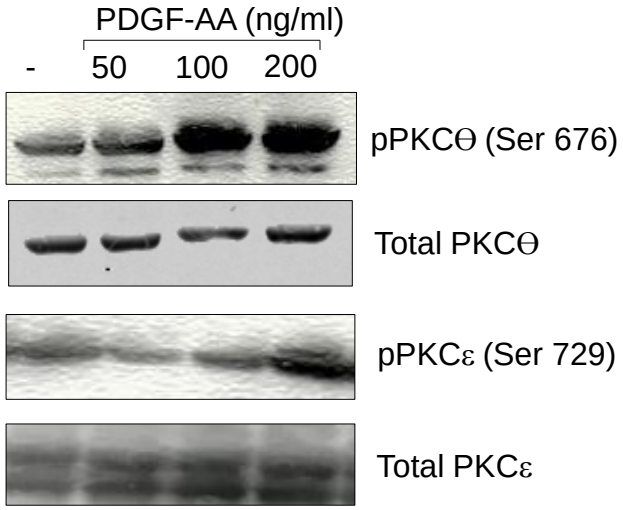
PDGF-AA (ng/ml)
-
50
100
200
pPKCΘ (Ser 676)
Total PKCΘ
pPKCε (Ser 729)
Total PKCε

Fig. 4

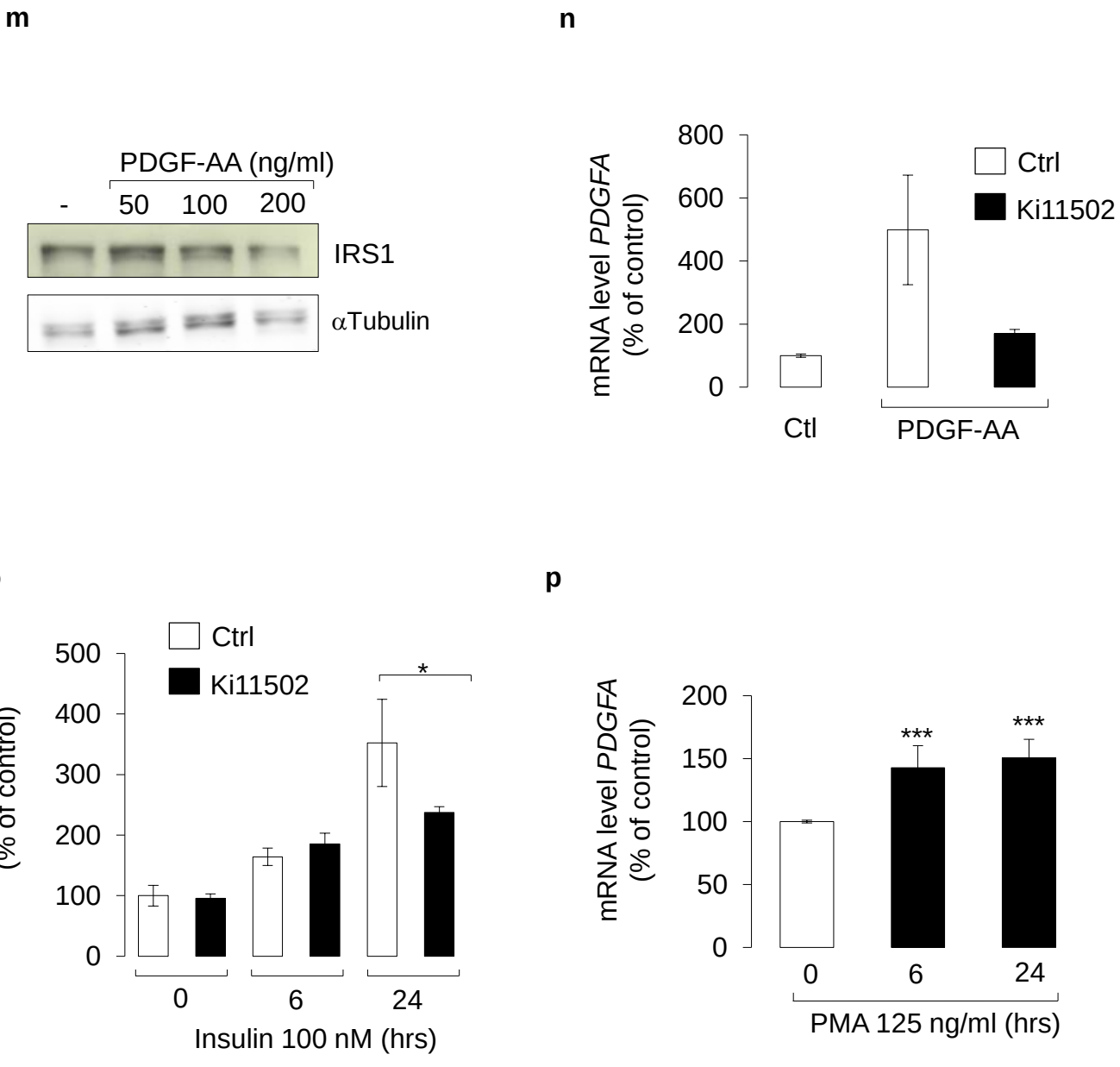
m
PDGF-AA (ng/ml)
-
50
100
200
IRS1
αTubulin
n
mRNA level PDGFA (% of control)
800
600
400
200
0
Ctrl
Ki11502
Ctl
PDGF-AA
o
mRNA level PDGFA (% of control)
500
400
300
200
100
0
Ctrl
Ki11502
*
0
6
24
Insulin 100 nM (hrs)
p
mRNA level PDGFA (% of control)
200
150
100
50
0
***
***
0
6
24
PMA 125 ng/ml (hrs)

Fig. 4

q

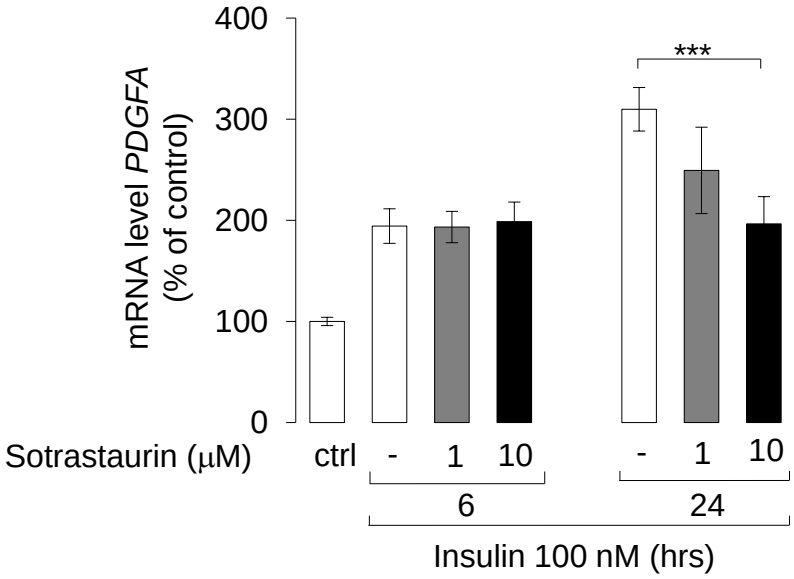
400
300
200
100
0
mRNA level *PDGFA* (% of control)
***
Sotrastaurin (μM)
ctrl
-
1
10
-
1
10
6
24
Insulin 100 nM (hrs)

r

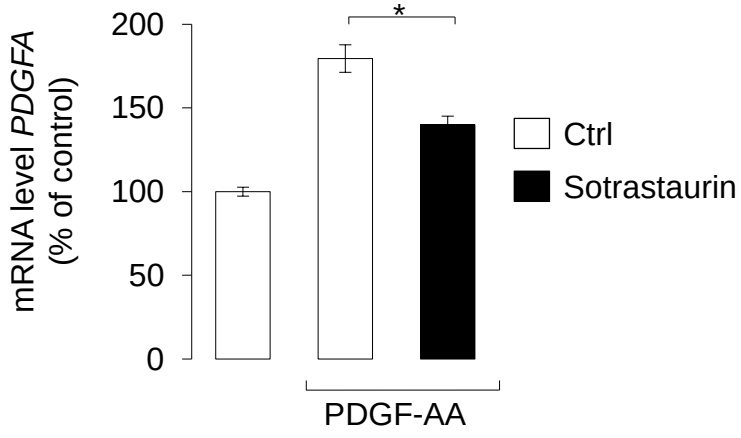
200
150
100
50
0
mRNA level *PDGFA* (% of control)
*
Ctrl
Sotrastaurin
PDGF-AA

Fig. 4

s

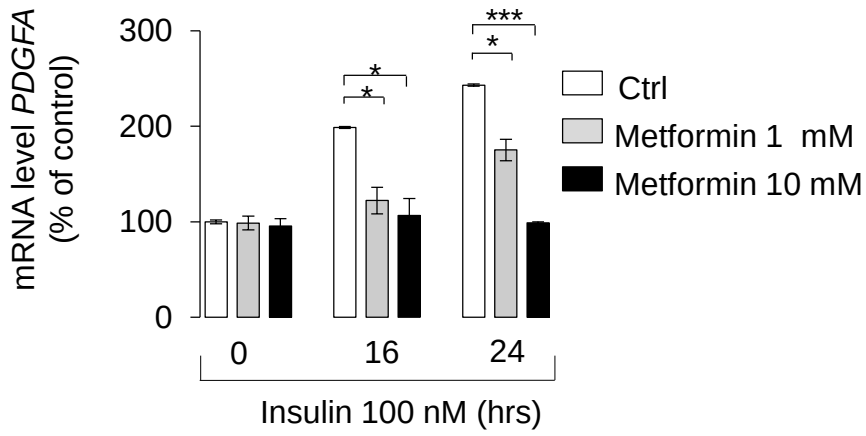
mRNA level *PDGFA* (% of control)
300
200
100
0
*
*
***
*
Ctrl
Metformin 1 mM
Metformin 10 mM
0
16
24
Insulin 100 nM (hrs)

t

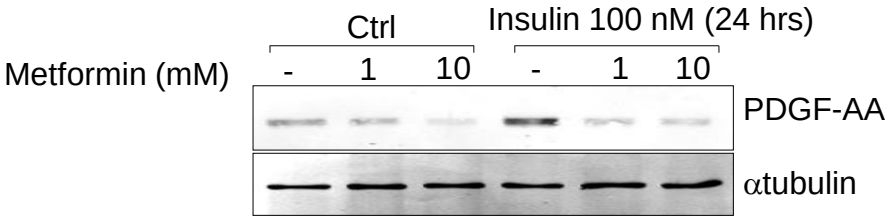
Ctrl
Insulin 100 nM (24 hrs)
Metformin (mM)
-
1
10
-
1
10
PDGF-AA
αtubulin

u

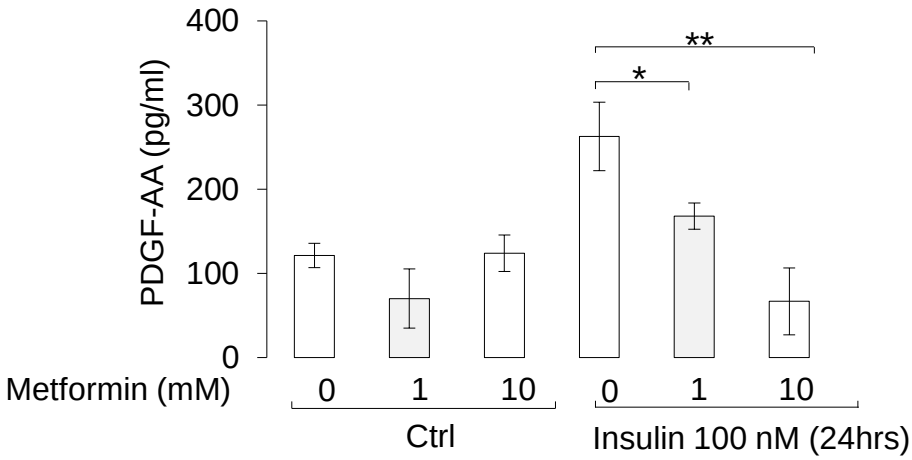
PDGF-AA (pg/ml)
400
300
200
100
0
**
*
Metformin (mM)
0
1
10
0
1
10
Ctrl
Insulin 100 nM (24hrs)

Fig. 5

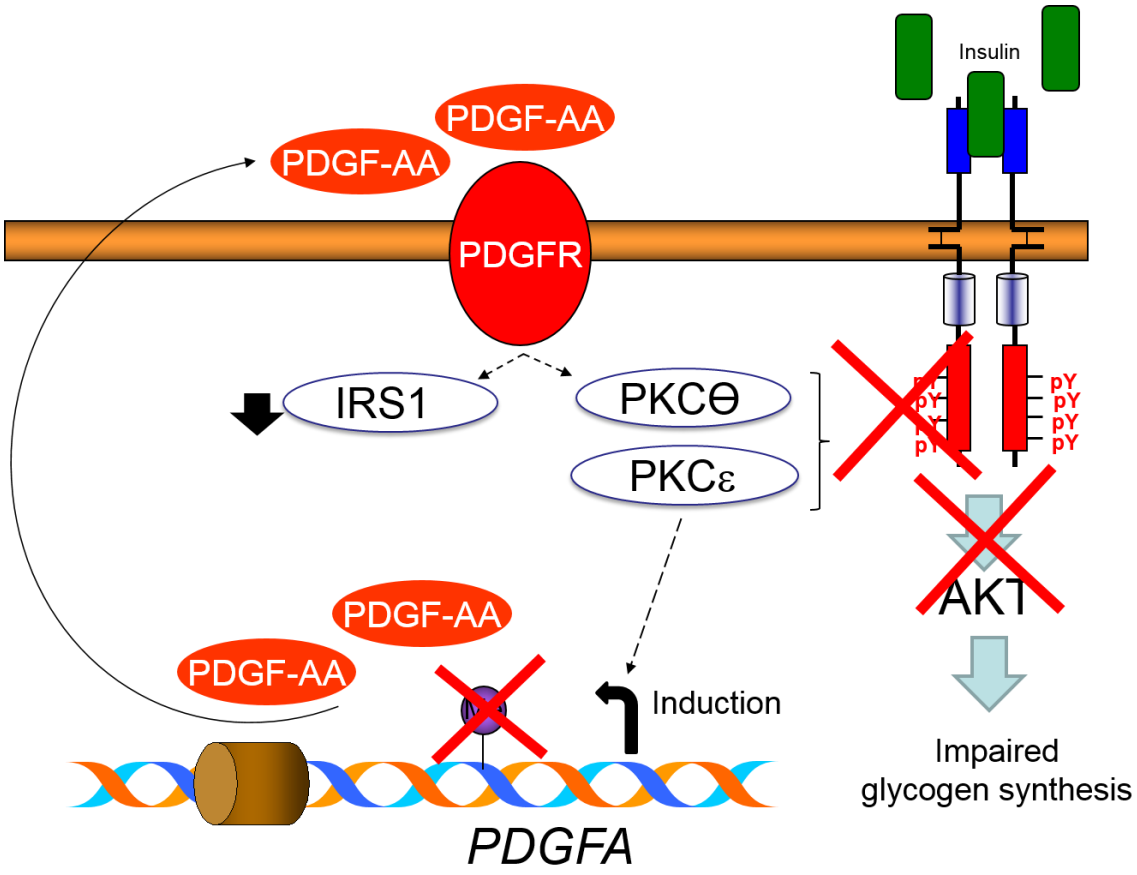
Insulin
PDGF-AA
PDGF-AA
PDGFR
IRS1
PKCΘ
PKCε
pY
pY
pY
pY
AKT
PDGF-AA
PDGF-AA
Induction
PDGFA
Impaired
glycogen synthesis